Advances in the physics studies for the JT-60SA tokamak exploitation and research plan

G. Giruzzi[1], M. Yoshida[2], N. Aiba[2], J.F. Artaud[1], J. Ayllon-Guerola[3], O. Beeke[4], A. Bierwage[2], T. Bolzonella[5], M. Bonotto[5], C. Boulbe[6], M. Chernyshova[7], S. Coda[8], R. Coelho[9], D. Corona[9], N. Cruz[9], S. Davis[10], C. Day[11], G. De Tommasi[12,13], M. Dibon[14], D. Douai[1], D. Farina[15], A. Fassina[5], B. Faugeras[6], L. Figini[15], M. Fukumoto[2], S. Futatani[16], K. Galazka[7], J. Garcia[1], M. Garcia-Muñoz[3], L. Garzotti[17], L. Giudicotti[5], N. Hayashi[2], M. Honda[2], K. Hoshino[18], A. Iantchenko[8], S. Ide[2], S. Inoue[2], A. Isayama[2], E. Joffrin[1], Y. Kamada[2], K. Kamiya[2], M. Kashiwagi[2], H. Kawashima[2], T. Kobayashi[2], A. Kojima[2], T. Kurki-Suonio[19], P. Lang[14], Ph. Lauber[14], E. de la Luna[20], G. Marchiori[5], G. Matsunaga[2], A. Matsuyama[21], M. Mattei[12,13], S. Mazzi[22], A. Mele[12,13], Y. Miyata[2], S. Moriyama[2], J. Morales[1], A. Moro[15], T. Nakano[2], R. Neu[14], S. Nowak[15], F.P. Orsitto[12], V. Ostuni[1,23], N. Oyama[2], S. Paméla[17], R. Pasqualotto[5], B. Pégourié[1], E. Perelli[15], L. Pigatto[5], C. Piron[24], A. Pironti[12,13], P. Platania[15], B. Ploeckl[14], D. Ricci[15], M. Romanelli[17], G. Rubino[25], S. Sakurai[2], K. Särkimäki[19], M. Scannapiego[11], K. Shinohara[2], J. Shiraishi[2], S. Soare[26], C. Sozzi[15], T. Suzuki[2], Y. Suzuki[27], T. Szepesi[28], M. Takechi[2], K. Tanaka[27], H. Tojo[2], M. Turnyanskiy[29], H. Urano[2], M. Valisa[5], M. Vallar[5], J. Varje[19], J. Vega[20], F. Villone[12,13], T. Wakatsuki[2], T. Wauters[30], M. Wischmeier[14], S. Yamoto[2], R. Zagórski[7]

[1] *CEA, IRFM, F-13108 Saint-Paul-lez-Durance, France.*
[2] *National Institutes for Quantum and Radiological Science and Technology, Naka, Ibaraki, 311-0193, Japan*
[3] *University of Seville, 41012 Seville, Spain*
[4] *Rudolf Peierls Centre for Theoretical Physics, University of Oxford, UK*
[5] *Consorzio RFX, I-35127 Padova, Italy*
[6] *Université de Nice, Nice, France*
[7] *Institute of Plasma Physics and Laser Microfusion, Hery 23, 01-497 Warsaw, Poland*
[8] *EPFL, Swiss Plasma Center, CH-1015 Lausanne, Switzerland*
[9] *Instituto de Plasmas e Fusão Nuclear, Instituto Superior Técnico, Universidade de Lisboa, P-1049-001 Lisboa, Portugal*
[10] *Fusion for Energy, D-85748 Garching, Germany*
[11] *Institute for Technical Physics, Karlsruhe Institute of Technology, Karlsruhe, Germany*
[12] *Consorzio CREATE, Napoli, Italy*
[13] *Università degli Studi di Napoli Federico II, Napoli, Italy*
[14] *Max-Planck-Institut für Plasmaphysik, D-85748 Garching, Germany*
[15] *Istituto di Fisica del Plasma CNR, 20125 Milano, Italy*
[16] *Universitat Politècnica de Catalunya, Barcelona, Spain*
[17] *CCFE, Culham Science Centre, Abingdon OX14 3DB, UK*
[18] *Faculty of Science and Technology, Keio University, Yokohama, Kanagawa 223-8522, Japan*
[19] *Aalto University, Department of Applied Physics, Aalto, Finland*
[20] *Laboratorio Nacional de Fusion, CIEMAT, 28040, Madrid, Spain*
[21] *National Institutes for Quantum and Radiological Science and Technology, Rokkasho, Aomori, 039-3212, Japan*
[22] *Aix-Marseille University, CNRS, PIIM, UMR, 7345, Marseille, France*
[23] *Politecnico di Torino, Torino, Italy*
[24] *EUROfusion /ENEA, Centro Ricerche Frascati, Italy*
[25] *Università della Tuscia, Viterbo, Italy*
[26] *Institute of Cryogenics and Isotopic Technologies - ICIT, 240050, Rm. Valcea, Romania*
[27] *National Institute for Fusion Science, Toki, Gifu 509-5292, Japan*

[28]*Wigner Research Centre for Physics, Budapest, Hungary*
[29]*EUROfusion Programme Management Unit, D-85748 Garching, Germany*
[30]*Laboratory for Plasma Physics, LPP-ERM/KMS, Brussels, Belgium*

E-mail: gerardo.giruzzi@cea.fr

Abstract. JT-60SA, the largest tokamak that will operate before ITER, has been designed and built jointly by Japan and Europe, and is due to start operation in 2020. Its main missions are to support ITER exploitation and to contribute to DEMO machine and scenario design. Peculiar properties of JT-60SA are its capability to produce long-pulse, high-β and highly shaped plasmas. The preparation of JT-60SA Research Plan, plasma scenarios and exploitation is producing physics results that are not only relevant to the future JT-60SA experiments, but often constitute original contributions to plasma physics and fusion research. Results of this kind are presented in this paper, in particular in the areas of fast ion physics, high-beta plasma properties and control, non-linear ELM stability studies.

1. Introduction

JT-60SA is a fully superconducting tokamak device jointly designed, built and in the near future exploited by Japan and Europe under the Broader Approach Satellite Tokamak Programme, and under the Japanese national programme. It is the largest tokamak ever built before ITER and due to start operation in 2020 [1]. Both before and during the D-T phase of ITER, it will exploit and extend the legacy both of JET and of the superconducting tokamaks presently in operation (WEST, EAST, KSTAR). The main missions of JT-60SA are: i) to support the ITER experimental programme as a satellite machine; ii) at the same time, to pave the way to the next step of the international fusion programme, i.e., the demonstration fusion reactor (DEMO). More specifically, JT-60SA should provide key elements for the choice of DEMO parameters and the design of DEMO scenarios, in particular for a steady-state, advanced performance design option. In addition to the large size (allowing high current and energy confinement), JT-60SA has been conceived with the main capabilities required to accomplish these missions: high β (the ratio of kinetic to magnetic pressure), high shaping, long pulse, high-power and flexible heating and current drive system, dedicated magnetic coils to provide adequate control of scenarios close to the performance limits.

The construction and assembly phase of the machine has been accompanied by the preparation of an extensive Research Plan [2], describing the various phases of the machine exploitation, in line with its progressive upgrades. This elaboration has been paralleled by a number of coherent physics studies aiming at preparing a sound basis for the scientific exploitation of the machine [3]. They involve advanced modelling connected with the priorities of the scientific programme; conceptual studies of diagnostics and other sub-systems to improve the quality of the experiments; development and validation of operation oriented tools. The preparation of JT-60SA exploitation has served as a catalyser leading to the production of physics results that are not only relevant to the future JT-60SA experiments, but often constitute original contributions to plasma physics and fusion research, which are summarised and briefly described in this paper. The focus of these studies can be defined as the sustainment and control of high-β long-pulse discharges in various plasma regimes. This requires a number of tools that have been studied and developed systematically:

- global discharge simulation and integrated scenario modelling of its phases
- wall conditioning (preparatory and inter-pulse)
- breakdown and current ramp-up
- flat-top sustainment and control (core and edge profiles, fast ions, power loads)
- control and mitigation of instabilities and disruptions

For each one of these elements, modelling studies have been carried out, but also specific projects of new machine sub-systems have been launched and are being carried out by EU and Japanese teams for use in the commissioning and/or in the subsequent experimental campaigns. In some cases, preparatory experiments and tests have been carried out in EU devices. In this paper the ensemble of these studies and the contribution they give to the sustainment and control of high-β long-pulse discharges in JT-60SA will be summarised, but specific highlights will be given on the most recent and advanced results.

The plan of the paper is the following: in Sec. 2 the characteristics of the JT-60SA tokamak and the main elements of its experimental programme are shortly presented. In Sec. 3, research advances towards controllable high-β, long-pulse scenarios in JT-60SA are described. Conclusions and prospects are presented in Sec. 4.

2. The JT-60SA tokamak and experimental programme

An extensive description of the JT-60SA device and actuators characteristics can be found in Refs. [1-4] and they are briefly summarised here. The machine has been conceived in order to attain high plasma performance and fully non-inductive discharges, not only through large size and high H&CD (heating and current drive) systems, but also through a high and flexible shaping capability. The main parameters are shown in Table 1. Optimisation of the aspect ratio (A~2.5) and shaping factor $S = q_{95}I_p/(aB_t) \sim 7$ (where I_p is the plasma current, B_t the toroidal magnetic field, a the minor radius and q_{95} the safety factor at 95% of the magnetic flux), in connection with the machine missions, have been key elements of the design, as well as the possibility of varying the plasma shape, from single-null to double-null, including an ITER-like shape. The machine characteristics allow performing discharges in the three main ITER regimes, i.e., H-mode at high current (5.5 MA), advanced inductive (hybrid) and steady-state at lower current. A set of reference scenarios has been developed and is described in [2]. Their main parameters are displayed in Table 2.

Non-inductive current drive (CD) is provided by the 10 MW negative-ion based neutral beam system (N-NBI) and by the 7 MW electron cyclotron (EC) waves system. Strong plasma heating by the 24 MW positive-ion based neutral beam system (P-NBI) is of course also an essential ingredient of the CD capabilities, via the bootstrap current associated to the pressure gradient. Part of the P-NBI power is injected tangentially, in the co-current (4 MW) and in the counter-current (4 MW) directions, allowing toroidal rotation control, which has a significant impact on plasma confinement and performance. The heating system also allows flexible sharing of the ion and electron heating, a crucial parameter for plasma transport properties. For power loads and density control, several generations of plasma facing components (PFC) and in particular of divertors, are foreseen, with increasing capabilities of power flux (up to 15 MW/m^2) and energy removal, eventually allowing full power discharges for 100 s current flat-top duration. Transition from carbon based to tungsten based PFC is foreseen after ~10 years of machine operation.

Control of plasma shape, position, error fields and main MHD instabilities will be ensured by the characteristics of the equilibrium field coils, by an extensive set of in-vessel coils and by the ECCD (Electron Cyclotron Current Drive) system. In particular, control of the instabilities peculiar to high-β regimes, i.e., NTM (neoclassical tearing modes) and RWM (resistive wall modes) will be crucial for the machine missions. Density control is essential for

long pulse regimes and will be provided by a divertor cryopump system [5] for pumping and, for matter injection, by gas puff and pellet injection [6], which is also used for Edge Localised Modes (ELM) pacing. An extensive set of diagnostics, for both control and scientific exploitation purposes, will be available and upgraded in the various phases of the machine exploitation, as described in the Appendix D of [2].

JT-60SA is now in an advanced phase of assembly, as shown by Fig. 1, and is due to start operation in 2020. The various research phases of the machine life are extensively discussed in [2]: the machine integrated commissioning will be carried out with Hydrogen plasmas; this part of the Initial Research Phase will also include experiments aiming at risk mitigation for the Hydrogen phase of ITER. The following Initial Research Phase in Deuterium will explore the main ITER scenarios (H-mode and hybrid) and the advanced high-β scenario at progressively increasing heating power (up to 80% of the nominal power), but for relatively short pulses (~5s), compatible with the initial C-coated divertor set. Installation of a new divertor made of carbon fibre reinforced (CFC) monoblocks will allow the start of the Integrated Research Phase, in which all the high-performance scenarios will be investigated for long pulses (~100s flat-top duration) and heating power close to the nominal value, using active cooling. Extensive studies of high-β steady-state plasmas with optimum control strategies will be the main target of this phase. At this point, a major upgrade of the machine will be carried out, in which JT-60SA will become a fully metallic machine, with tungsten as plasma facing material. High performance scenarios combining high-density, high-β, little or no-ELMs and highly radiative divertor will be developed in this new configuration, in direct support to the contemporary ITER D-T experiments. Full exploitation of these scenarios (completely relevant to DEMO) will take place in the following Extended Research Phase, in which further optimisation of divertor shape will be attempted and the double null configuration will be explored. Disruption management strategies, essential for ITER, DEMO and future tokamak reactors, will be developed and tested during the whole machine exploitation.

3. Research towards controllable high-β, long-pulse scenarios

Systematic studies have been conducted with the main goal of preparing the scientific exploitation of JT-60SA, but also of identifying the characteristics of diagnostics and actuators that should be developed in view of an efficient research programme. Discussion of the research results obtained can be organised around the typical sequence of items that have to be

considered for the realisation of a successful high-β, long-pulse discharge: from global discharge preparation via simulation, to wall conditioning, breakdown, ramp-up, flat-top sustainment, MHD and disruption control. Highlights of the main recent results in these areas are described in the following sub-sections.

3.1 Discharge simulation and integrated scenario modelling

Predictive simulation of plasma discharges is the basis of experiment preparation and the preliminary step for other analyses: MHD stability, sub-systems performance, control strategies. Extensive scenario evaluation and preparation have been done using free-boundary equilibrium codes, such as ACCOME [7] (including NBI sources) and TOSCA [8]. Global discharge simulations, producing time evolution of all the physical quantities, including magnetic equilibrium and radial profiles, are better done by fast simulators and indeed systematic analyses have been carried out with the METIS code [9] and reported in [2]. A much more accurate evaluation can be done if limited to particular phases of the discharge, for instance the flat-top stationary phase, by integrated modelling codes, such as TOPICS [10], CRONOS [11] and JINTRAC [12]. In order to make such predictions as reliable as possible, a procedure for validation of models and benchmark of integrated modelling codes has been employed, based on a set of reference JT-60U and JET discharges, representing the main scenarios (H-mode, hybrid, advanced). These discharges have been predictively simulated using both Japanese and EU codes, with a variety of transport, pedestal, rotation models and scalings, with the aim of finding a unified modelling framework that works for the set of reference discharges of both machines, which are the most similar in size and characteristics to JT-60SA. In addition, this work has provided benchmark of the integrated modelling suites of codes employed, with satisfactory results, as reported in [13-15]. Various transport models have been tested and can be used with comparable accuracy for predictive simulation of most of the reference discharges. In particular, the CDBM heat transport model [16] provided accurate or, in some cases, conservative estimates of the electron and ion temperatures. A similar procedure is now being used for the current ramp-up phase [17].

On this basis, more complex phenomena can be analysed with the validated modelling framework. For instance, the formation of an ITB (Internal Transport Barrier), its compatibility and alignment with non-inductively driven currents, its controllability, which are basic ingredients of the steady-state high-β scenario 5 [2]. The CDBM transport model naturally allows ITB formation when the current density profile is peaked off-axis, as shown by the

TOPICS simulation presented in Fig 2. The strength of the ITB is found to be sensitive to the precise modelling of the N-NBI current drive, in this case performed by means of the orbit-following Monte Carlo code OFMC [18] and including finite orbit width effects. Control of the ITB location and strength can be performed by small variations of the N-NBI power and/or by additional ECCD, and evaluated by means of this type of simulations [19].

Another phenomenon that is going to play a relevant role in integrated scenario modelling is plasma rotation, because of the impact of rotation shear on heat transport and generally plasma performance. JT-60SA has a flexible tool to control toroidal rotation, i.e., the torque due to co- and counter-injected P-NBI at 85 keV. However, the plasma response has to be evaluated taking into account braking due to non-axisymmetric perturbations of the toroidal field, owing to ripple, error fields and intentionally applied resonant magnetic perturbations (RMP) that will be used for ELM control. In JT-60SA, these RMPs can be produced by the same system of coils that corrects error fields (EFCC), aimed at suppressing locked modes. The ensemble of these perturbations give rise to the so-called neoclassical toroidal viscosity (NTV), an effect that is not usually included in integrated scenario modelling. This has been accomplished by an advanced modelling framework [20] combining in an iterative way: TOPICS [10], OFMC [18] for the evaluation of the NBI induced torque, the 3D neoclassical code FORTEC-3D [21] and the 3D equilibrium code VMEC [22]. An example of the toroidal rotation computed by means of this modelling framework for a high-current (5.5 MA) H-mode scenario of JT-60SA is shown in Fig. 3. On the left panel, red, green and blue curves respectively display the profiles of toroidal rotation velocity without the NTV effect, with the NTV due to magnetic ripple and also including the effect of a n=3 RMP induced by 10 kA current in each of the EFCC, with even parity. On the right panel, the NTV torque (with and without RMP) is shown, together with the radial electric field. It is shown that significant braking is caused by the ripple and should be taken into account in integrated modelling simulations. On the other hand, the n=3 RMP at 10 kA (which is typically used for ELM control) has a modest effect on the toroidal velocity, meaning that ELM control will not be detrimental to plasma rotation. However, higher applied currents in the EFCC (~30 kA) will have stronger impact and could be effectively used for rotation control, as discussed in [20].

3.2 Wall conditioning, breakdown and current ramp-up

It is well known that plasma performance and discharge reproducibility in fusion machines strongly depend on the state of the walls, because of the impact of both main ion and impurity recycling. Recovery after disruptions usually needs particular care in order to have a

broad enough operation window for breakdown. Because of the superconducting magnetic field, glow discharge cleaning will not be usable in JT-60SA between shots (as in ITER) and Electron Cyclotron Wall Conditioning (ECWC) is envisaged, a technique that has been tested but not fully validated yet, in particular at the 2nd EC harmonic. In order to improve the knowledge of this technique, dedicated experiments [23] have been performed on the TCV tokamak, demonstrating that after dedicated Helium discharges with ECWC at the 2nd EC harmonic (extraordinary mode, X2), standard Ohmic Deuterium plasmas could be then sustained, whereas it would not have been possible without adequate wall conditioning. Discharge parameters on TCV were optimised to (i) minimise the absorption of EC stray radiation by in-vessel components by minimising the plasma breakdown time and maximising the absorption of power over the duration of the conditioning discharge, and to (ii) improve the discharge homogeneity and wall coverage, in particular towards the inboard surfaces where JT-60SA plasmas will be initiated. The main control parameters in this study are the addition of a poloidal magnetic field to the nominal toroidal field, the discharge pressure and the EC power. In order to extrapolate these results to future JT-60SA ECWC experiments and routine use, modelling has been carried out by means of the TOMATOR-1D code [24]. This 1-dimensional reaction-diffusion-convection code has been developed to simulate plasma production by radio-frequency waves inside a tokamak, using the Braginskii continuity and heat balance equations. In this algorithm, the evolution of the radial density and temperature profiles is documented for 9 species for H_2/He/C plasma mixtures from a transient to a steady state condition. The plasma simulator is used to study EC absorption and transport properties as a function of the applied vertical magnetic field component. Figure 4 shows the experimental electron density measured by Thomson scattering on TCV at $\omega = 2\omega_{c,e}$ and the simulated density by TOMATOR-1D for X2-ECRH plasma at 1.5T, 400kW of launched power, toroidal and poloidal injection angle of 19.3° and 7.0° respectively. The simulations, reproducing the experimental data, predict Bohm like diffusion transport, convection losses of the order of 10-100 m/s and an EC absorption scaling proportional to $P_{abs}/P_{in} \propto n_e T_e$ as predicted by the quasi-optical beam tracing code GRAY [25]. The dependence of transport processes on the vessel dimensions via a multi-machine study is required to arrive at predictive capabilities for ECWC plasma on JT-60SA.

Breakdown and plasma initiation is a particularly delicate phase in a new machine, operating with a new control system. Assistance by EC waves for pre-ionisation and plasma heating to burnthrough can prove essential to improve the efficiency of this task and will be

mandatory in ITER [26]. Predictive modelling of EC-assisted breakdown could significantly speed up the search for optimised breakdown configurations, however it requires a complex simulation framework, combining free-boundary equilibrium equations, balance equations for the time evolution of energy and particles (with ionization/recombination terms and impurities) together with the circuit equation for the plasma current, and EC wave propagation equations, including at least the first wall reflection. To this end, a dedicated modelling workflow has been developed and is being validated on experiments [27]. It combines the breakdown code BKD0 [28], the beam-tracing code GRAY [25] and CREATE-BD, a specific version of the free-boundary equilibrium code CREATE [29], which integrates and optimises the active circuit currents, taking into account eddy currents in the passive structures for developing the plasma breakdown scenario. Furthermore, the BKD0 impurity model, consistent with the code DYON [30] for carbon wall machines, has been validated on TCV experiments. Several cases have been treated, for the two main frequencies of the JT-60SA gyrotrons: 110 GHz and 138 GHz [31], the additional operation frequency of 82 GHz, and various injection angles. The electron temperature and plasma current depend on ECRH power and present a threshold for successful start-up. Figure 5 shows this computed EC power threshold as a function of the initial neutral H_2 pressure for two cases: (i) 138 GHz (2^{nd} harmonic) X-mode, injection perpendicular to the magnetic field and at fixed poloidal angle 35.5° with respect to the horizontal direction (blue curve) and (ii) 82 GHz (1^{st} harmonic) O-mode, optimised injection angles (green), i.e., poloidal angle 21° and toroidal angle (with respect to the perpendicular) of 20°. For this second case, two different values of the initial C content and oxygen fraction n_O/n_H=0.1% have been considered. As the initial pressure increases, more power is required to overcome the radiation barrier. The steerable launcher that will equip JT-60SA after the commissioning phase will allow optimising the absorption and increase the operational space even in presence of impurities: the main difference between the two cases is related to the fact that injection angle optimisation by means of a steerable launcher allows second pass after the first reflection through the initial small plasma, with change of polarisation from O to X mode, which greatly increases the EC wave effect owing to substantial increase in the second pass absorption.

In order to monitor this delicate phase (as well as for general plasma overview) a wide-angle version of the EDICAM visible camera [32] has been designed and manufactured as a direct European contribution to JT-60SA diagnostics. It will be an important tool for detection of dangerous events, such as hot-spots, plasma boundary identification with a temporal resolution up to 1 kHz (comparable to magnetic equilibrium reconstruction), disruptions, SOL

statistical properties etc. Moreover, this will be the phase in which the machine could be more likely prone to risks connected with EC stray radiation, owing to incomplete absorption of the EC wave beams. This has motivated specific studies [33-34], in which an analysis of the residual non-absorbed ECRF power fraction expected in the various applications and plasma scenarios has been carried out, studying its dependence on the steering angle and on the plasma main parameters such temperature and density. Both transient conditions, such as plasma start-up, and flat-top scenarios have been taken into consideration. Moreover, the expected stray power density distribution in the vessel and particularly around the potentially critical areas such as diagnostics windows or pumping ducts has been evaluated. An adequate detection system to limit the risks related to stray radiation is presently considered.

After breakdown and burnthrough are obtained, the current and density ramp-up is a crucial phase for the establishment of high-performance scenarios while saving central solenoid flux: X-point formation, high shaping control, H-mode transition and in particular the access to safety factor profiles typical of JT-60SA advanced regimes (hybrid and steady-state). Earlier simulations of this phase have been performed with the MECS code [35-36] and benchmarked [37] with the CREATE-NL code [38]. A way to improve the accuracy of this type of simulations is to couple a free-boundary equilibrium code with a plasma model including the main ingredients of integrated modelling, i.e., heat and particle transport, current diffusion, H&CD modules. Although some examples of such a code coupling exist in the literature, the required computation time is usually extremely large. In order to keep it at a level that makes this type of modelling practical and useful for preparing experimental scenarios, the fast integrated modelling code METIS [9] is used as plasma module and has been coupled to two different free-boundary equilibrium codes, for alternative uses: CREATE-NL [38] and FEEQS [39]. FEEQS is used in inverse mode in conjunction with METIS to compute the pre-magnetisation phase and to initialise and optimise the plasma scenario, verifying the coils limits. An example is given in Fig. 6, showing three snapshots of free-boundary equilibria computed by FEEQS (top) and the self-consistent evolutions of the poloidal beta β_{pol}, internal inductance l_i, electron temperature and current density profiles computed by METIS (bottom). Full simulation including controllers can be performed by means of CREATE-NL exchanging equilibrium and profiles data with METIS in the framework of a SIMULINK scheme.

3.3 Flat-top plasma sustainment: density, power loads, radiation

Density control is a key ingredient for long pulse regimes and in particular for access to high density scenarios, close to the Greenwald limit. The two main actuators of such control

will be the divertor cryopump system [5] and the pellet fuelling system, which is being designed [6]. This will be an advanced system, conceived for combined fuelling and ELM pacing using two extruders. Detailed modelling of pellet ablation, using the HPI2 code [40], has been carried out in order to determine the optimum pellet injection location and parameters for all the reference scenarios and optimise the system design. The same code has been used in conjunction with the integrated modelling suite JINTRAC, appropriately set-up for JT-60SA simulations [15], in order to assess the feasibility of combined fuelling and ELM pacing. The JINTRAC simulation starts from parameters typical of scenario 2 (see Table 2) and models the growth of the density due to the injection of trains of pellets with frequency 12.5, 11.1, 10.0, 9.1, 8.3 and 7.7 Hz respectively. The pellets are injected every 5 s, which allows attaining nearly stationary densities. In addition, ELM pacing pellets at 50 Hz are injected between fuelling pellets. This corresponds to the injection patterns of two centrifuge arms rotating at 50 Hz with a fuelling pellet injected every 4, 4.5, 5, 5.5, 6 and 6.5 rotations respectively. The pellet injection velocity was set to 400 m/s and the masses of the fuelling and ELM pacing pellets are 6.5 10^{20} atoms and 0.8 10^{20} atoms respectively. The results for the case with fuelling pellets only are shown in Fig. 7. The electron density profile vs time and normalised radius is shown in the top panel and the electron temperature in the bottom panel. It can be seen that it is possible to increase the density from the level characteristic of scenario 2 to significantly higher density (typical of scenario 3) within a few seconds. After the fast initial transient, a slow decrease of the average density is also seen as the pellet injection frequency is gradually reduced. In the corresponding case with simultaneous fuelling and ELM pacing pellets, there is an additional contribution by the pacing pellets that increases the density by 25-30% [6], as shown in Table 3. This contributes significantly to the fuelling of high-density scenarios and should be taken into account in the global control strategy of the discharge.

The second key element for long pulse regimes is the control of power loads on the divertor during the strong heating phase, which can be attained by divertor radiation associated with controlled impurity seeding strategies. Systematic studies of the relevant scenarios, but in a simplified geometry, have been performed by means of the COREDIV code, both for C-PFC [41-43], and W-PFC [42,44]. Simulations combining core, Scrape-Off Layer (SOL) and divertor have been performed for a scenario similar to Scenario 5-1, but at reduced heating power, using JINTRAC coupled to the edge code EDGE2D and the Monte Carlo code for the neutrals EIRENE [45]. Comparison of COREDIV and EDGE2D Carbon radiation patterns for Scenario 3 (high density) are shown in Fig. 8. In the case of EDGE2D-EIRENE the boundary

conditions on the core side are taken from the COREDIV results. Beside the employment of real geometry, EDGE2D-EIRENE treats neutrals with a Monte Carlo approach whereas COREDIV assumes the shape of neutrals distributions by analytical formulas, described by several parameters, like ionization length or recycling coefficient. Starting parameters were set as similar as possible for both codes: transport coefficients in the SOL (and around the pedestal) are the same ($\chi_{e,SOL}$=0.5 m^2/s, $\chi_{i,SOL}$=1.0 m^2/s, all particle diffusion coefficients 0.5 m^2/s). With these benchmark conditions, the total C radiation in the SOL and the remaining power delivered to the divertor target computed by the two codes are found to agree within 10%. The codes agree also on the overall C radiation distribution, both showing that the C SOL radiation will be concentrated in a region in the vicinity of the target plate. The reason underlying the differences of the radiation patterns are the aforementioned simplifications of COREDIV. The radiation pattern in Fig. 8 for EDGE2D-EIRENE follows the shape of a divertor leg (inner and outer), which obviously cannot be found in COREDIV due to the rectangular grid with a single target. However, as the figure uses logarithmic colour scale, the differences in the areas "below" yellow are irrelevant. Importantly, the different plasma conditions close to the targets (n_e and T_e, not shown) have severe impact on detachment; whereas COREDIV cannot correctly assess detachment and does not predict it indeed, EDGE2D-EIRENE exhibits full detachment when the electron density at the separatrix is increased to 3.6×10^{19} m^{-3}. Here, the dominant factor is the employed neutral model.

More sophisticated edge/SOL/divertor simulations have been performed by means of the SONIC code [46], extended to include multiple impurity species and impurity-impurity interaction, such as the physical sputtering of C by seeding impurities [47]. This allowed comparative simulations of the radiation patterns with C and injected Ne, Ar or mixtures. Simulations for the future JT-60SA phase with W-PFC using the highly sophisticated SOLPS-ITER code [48] are presented in [49]. In order to monitor the impurity levels in the divertor region, a new VUV spectrometer with imaging capability is under development [50].

3.4 Flat-top plasma sustainment: fast ions

Once the flat-top phase is attained, its sustainment for long pulses requires adequate current drive systems. On JT-60SA, non-inductive current will be mainly provided by the 500 keV N-NBI system (10 MW), with a limited additional contribution by the EC waves (7 MW). Of course, a substantial fraction of non-inductive current will be provided by the bootstrap current (estimated at 25 to 80%, depending on the reference scenario [2]) which is in turn mainly sustained by the ensemble of the heating systems, of which the most powerful is the 85

keV P-NBI one (24 MW). As a consequence, all the reference JT-60SA scenarios will be characterised by two substantial populations of fast ions, with different energy and pitch-angle parameters, driving different sets of Alfvénic instabilities. This is the most distinctive feature of the physics that will be accessible on this tokamak, not only for its potential interest for ITER and DEMO, but for the control and sustainment itself of the scenarios. In particular, the super-Alfvénic speed of the N-NBI driven fast ion population will be a unique feature before operation of the N-NBI system of ITER (1 MeV). The distribution functions of fast ion populations are accurately computed by means of Monte Carlo codes for various JT-60SA scenarios [51,52], as they can affect the global MHD stability of the discharge [53,54], turbulence properties [55] and therefore, non-linearly, the establishment of pressure and current density profiles. Measurement of the energy and pitch-angle distribution of the lost fast ions is particularly important in order to understand the physics mechanisms governing such a loss, which is also of key importance for the alpha particle confinement in ITER and DEMO. This has motivated the development of a fast ion loss detection system for JT-60SA, which is being designed [56,57] and will be installed for the high-power phase of the machine programme.

In addition to the detailed analysis of the Alfvén eigenmode stability (AE) and related energetic particles (EP) transport of single time slices [53], also faster tools for a survey-type analysis are needed for scenario modelling and optimisation. An automated workflow wrapper around the linear-gyrokinetic code LIGKA [58,59] has been developed in order to process many different equilibria in a reasonably short computation time (typically 1-3 min per equilibrium for 10 toroidal mode numbers, trivially parallelisable). A hierarchy of reduced models can be chosen (local/global, analytical/numerical coefficients for velocity-space integrals). In Fig. 9 the local damping rates of all toroidal Alfvén eigenmodes (TAE) with mode numbers n=1-10 (colour code), including Landau damping and a model for radiative damping, are shown as function of the on-axis safety factor q_0 (as model for current profile evolution during current ramp-up). Due to off-axis NB heating, the steepest EP gradients are expected between ρ=0.2-0.4 (positive EP gradient) and ρ =0.5-0.6 (negative EP gradient) [2]. Clearly, inner core TAEs are less damped compared to outer core TAEs, and different q-profiles favour the stability of different toroidal mode numbers. Adding energetic ions (modelled as a hot Maxwellian with an equivalent EP-pressure) leads to the stability diagram plotted in Fig. 10. Here the scenario parameters are taken from the CRONOS simulation of the hybrid scenario presented in Ref. [13], in which the EP distribution has been computed by the NEMO/SPOT Monte Carlo module. According to these simulations, for the hot Maxwellian a ratio of the EP to the thermal ion pressure is ~5 is

assumed. Again inner core (left) and outer core (right) TAEs are separated. For many values of q_0, no unstable modes are predicted in the outer core, and all growth rates are small. Moreover, typically only one toroidal mode number is unstable for a certain q_0 leading to the conclusion that the radially outward EP transport is negligible in this case. The core TAEs are more unstable (note that the local model tends to overestimate the growth rates), but depending on q_0, equilibria with either many unstable TAEs (q_0~1.22), or a few marginally unstable TAEs (q_0~1.4) or only stable TAEs (q_0~1.5) can be found. This sensitivity with respect to q_0 has been found in many present-day experiments [60-62] and is reproduced by the LIGKA model. Based on this fast analysis, a set of profiles can be chosen for in-depth analysis in order to guide the experimental and numerical search for stable, marginally stable or unstable (EP transport studies) TAE regimes.

3.5 MHD instabilities and transient events control

Controllability of JT-60SA scenarios will require avoidance or prompt reaction to a number of MHD instabilities and transient events, both in the stationary and in the ramp-up, ramp-down phases. Preparation of adequate control strategies has to be supported by deep understanding of the physical phenomena involved, in view of future application to ITER and DEMO. A distinctive example is the issue of disruptions, which should be accurately predicted, if possible avoided, and otherwise mitigated. This motivated the development of a disruption predictor for JT-60SA, which has undergone first tests on JT-60U data [63] and of a 2-valves Massive Gas Injection system [64] procured by EU and that will be available after the machine commissioning phase.

ELM studies. Not only disruptions should be avoided or mitigated in ITER and DEMO, but also ELMs: the search for no-ELM or small-ELM regimes is one of the main objectives of the JT-60SA programme. Such regimes have been found empirically, but first-principle simulation of the non-linear ELM dynamics is fundamental to gain insight into the conditions for the access to these regimes or for active ELM control. To this end, the 3D non-linear MHD code JOREK [65,66] has been applied to H-mode JT-60SA scenarios. The model contains all pedestal-relevant plasma flows, including two-fluid diamagnetic effects, neoclassical poloidal velocity and toroidal rotation. Linear stability has first been benchmarked with the linear MINERVA-DI code [67], then non-linear simulations have been performed for ballooning mode numbers n = 4-22 and various values of the plasma resistivity. Simulations start with a collapsed pedestal, which then builds on, until a ballooning mode becomes unstable and the ELM crash is produced. The obtained 2D pattern of the density for Scenario 4-1 is shown in Fig. 11. The

filamentary structures observed display the crash of a large ELM, corresponding to an energy loss ~12% of the total plasma energy content.

A method to limit the ELM size and make their crashes less harmful for the PFC is to induce ELMs of smaller amplitude on purpose, but more frequently (ELM pacing). This can be done by injecting pellets at a frequency higher than that required for plasma fuelling, as discussed in Sec. 3.3. The JOREK code has been used in the past to simulate the 3D density structures generated by pellet injection, e.g., for DIII-D and ITER [68], using the NGS code [69] as a module to compute the pellet ablation process. The same codes have been applied to simulate the effect of pellet injection on the 4-1 scenario of JT-60SA. Figure 12 shows the density contour plot in the poloidal cross section during the injection of a 0.8×10^{20} Deuterium pellet with velocity 470 m/s (pacing pellet). The localization of the density perturbation caused by the pellet injection is observed close to the injection point. Then the pellet cloud propagates along the magnetic field lines and reaches the top and the bottom of the plasma. Therefore, density perturbations in those regions are also observed, with filaments due to the ballooning mode structures. Considering that the mechanism of the pellet triggered ELM is due to the three-dimensionally localized pressure perturbation, it is important to study the pellet triggered ELM with a non-linear 3D MHD code such as JOREK. Another proven way of mitigating or suppressing ELMs is the use of resonant magnetic perturbation by magnetic coils. This can be done on JT-60SA by using the Error Field Correction Coils, as mentioned in Sec. 3.1.

RWM studies. High β_N scenarios are on one hand desirable for plasma performance but on the other hand challenging from the point of view of stability. In the JT-60SA Scenario 5 in particular, Resistive Wall Modes are predicted to be simultaneously unstable by ideal MHD modeling [70]. It is foreseen that synergetic contributions from passive (i.e. drift-kinetic resonances) and active means shall be exploited for RWM stabilisation. In JT-60SA, feedback control of RWMs will be possible thanks to a set of 18 active coils located on the inner side (i.e. the plasma facing side) of the Stabilizing Plate (SP), shown in Fig. 13 (left panel). A plasma response mode provided by the CarMa code [71] has been implemented for simulations of RWM feedback control with the most unstable n=1 and n=2 modes, where n is the toroidal mode number [72]. This model includes a realistic description of the active coils, with both RWM Control Coils (RWMCC) and Error Field Correction Coils (EFCC) represented as single turn conductors. The stabilizing plate is also described with all its 3D features, while an axisymmetric vacuum vessel is assumed. This is enough to introduce a significant degree of realistic detail, since the stabilizing plate is the closest conducting structure interacting with the

RWMs (r/a ~1.2, where a is the minor radius). The structure of an n=1 eigenmode computed by the CarMa code on an axisymmetric surface in the stabilizing plate position is shown in Fig. 13 (right panel). The 3D features of the stabilizing plate however introduce a destabilising effect and a splitting of the modes into multiple unstable eigenvectors. For this reason, ongoing work is aiming at developing a multimodal simulator for RWM control [72].

Energetic particles, an ubiquitous element of the JT-60SA high performance scenarios, are also expected to have an impact on RWM dynamics. In order to study these effects, a hybrid kinetic-MHD model has been developed and extended to include both energetic particles and toroidal plasma rotation in the MINERVA/RWMaC code [73]. The case of scenario 5-1 (high beta steady-state) has been considered, in particular to analyse the effect of the NBI parameters on the RWM stability: the injected beam energy E_a and the ratio of the parallel to the total velocity of the injected beam $v_{//}/v$ (pitch-angle parameter). Computed growth rates normalised to the wall decay time vs pitch-angle parameter of the injected Neutral Beam are shown in Fig. 14, with and without energetic particle rotation effect. The top panel shows the case of a low-energy beam (E_a = 100 keV), whereas the case of a high-energy beam (E_a = 500 keV) is shown in the bottom panel. In general, the energetic particle rotation effect causes a significant reduction of the mode growth rate, with the formation of new stable regions. This stabilising effect is attributed to non-resonant interaction between the rotating energetic particles and the mode.

NTM studies. NTMs are expected to be excited in virtually all the JT-60SA scenarios at nominal heating power, because JT-60SA reference scenarios will naturally attain high normalised β values (see β_N in Table 2). Their active control is one of the main functions of the ECCD system, which has been designed with the capability of providing the two main ingredients for NTM control: i) capability of driving localised currents at the main rational surfaces locations where NTMs are expected (i.e. q=3/2 and q=2); ii) modulation capability in the kHz range. In order to predict the EC power required for NTM reduction or suppression, the effect of ECCD with the actual design of the antenna configuration has being investigated by solving the Generalized Rutherford Equation [74], where several terms affecting NTM stability (such as bootstrap, curvature, polarization, non-inductive driven current, heating, wall…) are included. Equations for the time evolution of mode phase and frequency [75] are also solved and the wave propagation, absorption and driven current are computed by the beam-tracing code GRAY [25]. All these elements are combined in a workflow [76] allowing systematic evaluation for the JT-60SA scenarios, as reported elsewhere [77]. Here the case of the 2/1 mode for scenario 2 is

illustrated by Fig. 15. The top panel shows the time evolution of the mode island width and rotation frequency with no EC power. Different saturation levels can be attained, depending on details of the equilibrium and profiles, therefore two values are displayed. It appears that large 2/1 islands can lock in a few seconds (rotation frequency going to zero). In the bottom panel, the impact of 3MW EC waves of frequency 138 GHz, injected at a toroidal angle of 14°, is shown for the case of an island which would saturate at w ~ 0.08 m. Full suppression is obtained both with continuous and modulated EC wave injection. Modulated ECCD is more efficient, because it allows localising the interaction at the island O-point, where co-CD is stabilising. Larger islands will require higher EC power, still within the 7 MW available on JT-60SA (3MW is rather the power available in the Initial Research Phase). These cases are extensively discussed in Ref. [77].

Disruption studies. If some of the operational limits are exceeded, a rapid growth of an MHD instability makes the plasma lose most of its thermal energy – the so-called Thermal Quench (TQ), during which a current density profile flattening takes place. Consequently, the plasma current increases, experiencing a spike, so that the magnetic energy in the plasma keeps approximately constant. Immediately after, the plasma cools down and its resistivity increases, so that the plasma current drops to zero (Current Quench, CQ) and this may cause the vertical position feedback to lose control of plasma, giving rise to a Vertical Displacement Event (VDE): this is also called “cold VDE”, since the plasma has lost its thermal energy. Due to this vertical motion, the plasma eventually hits the wall, injecting currents directly in the structures (halo currents). In other cases, the VDE takes place at full thermal energy content (“hot VDE”) and the TQ occurs later, when the plasma hits the wall. This type of event has been modelled using the CarMa0NL code [78], able of treating an axisymmetric plasma under the evolutionary equilibrium assumption, in the presence of three-dimensional conducting structures surrounding the plasma itself. In particular, to complete previous results [79], a case with no stabilising plate has been considered; the plasma is forced to move downwards with a 1 kA step in the in-vessel coil current, until it hits the wall, when the TQ occurs: the poloidal beta drops to negligible values in 3 ms. Immediately after, the CQ takes place, with a linear decay of plasma current to 0 in 12 ms. Figure 16 shows two snapshots of this event. With respect to previous results [79], due to the lack of the effect of the stabilizing plates, larger plasma displacements take place on short time scales.

4. Conclusions and prospects

The JT-60SA scientific programme is both broad and ambitious, as appropriate to a large and international experimental device that will be at the forefront of the international fusion programme for many years. The physics studies presented in this paper, although not an exhaustive description, provide relevant examples of the efforts necessary to build a physics basis for realising the main research objectives defined in the Research Plan [2]. Such studies will accompany the machine enhancement programme that will be developed in parallel with the operation and scientific exploitation phase. The most significant enhancement will be the transition to W-PFC, for which R&D is in progress, including tests of specifically developped W coatings [80]. Ideas of advanced diagnostics are developed for possible application in the integrated and extended research phases. For instance, in connection with the key objective of current profile control, conceptual design of a polarimetry system has been carried out [81]. In connection with turbulence studies, as, for instance, those reported in [82], turbulence diagnostics for both core and edge have been proposed and are being designed [83,84]. The forthcoming start of the machine operation (2020) is expected to further intensify these prospective studies.

Acknowledgements

This work has been carried out within the framework of the EUROfusion Consortium and has received funding from the EURATOM research and training programme 2014-2018 and 2019-2020 under grant agreement No 633053. The views and opinions expressed herein do not necessarily reflect those of the European Commission. The authors gratefully acknowledge members of the JT-60SA Integrated Project Team for data exchange and fruitful discussions.

References

[1] Barabaschi P et al. 2019 Nucl. Fusion **59** 112005

[2] JT-60SA Research Unit, *"JT-60SA Research Plan. Research Objectives and Strategy"*, v4.0, Sept. 2018, *http://www.jt60sa.org/pdfs/JT-60SA_Res_Plan.pdf*

[3] Giruzzi G, Yoshida M et al. 2017 Nucl. Fusion **57** 085001

[4] Kamada Y et al. 2011 Nucl. Fusion **51** 073011

[5] Luo X et al. 2018 Fusion Eng. Des. **136** 467

[6] Lang P et al. 2019 Fusion Sci. Techn. **75** 178 DOI: 10.1080/15361055.2018.1471960
[7] Tani K et al. 1992 J. Comp. Phys. **98** 332
[8] Shinya K 2000 J. Plasma Fusion Res. **76** 479
[9] Artaud J-F et al. 2018 Nucl. Fusion **58** 105001
[10] Hayashi N et al. 2010 Phys. Plasmas **17** 056112
[11] Artaud J-F et al. 2010 Nucl. Fusion **50** 043001
[12] Romanelli M et al. 2014 Plasma Fusion Res. **9** 3403023
[13] Garcia J et al. 2014 Nucl. Fusion **54** 093010
[14] Hayashi N et al. 2017 Nucl. Fusion **57** 126037
[15] Garzotti L et al. 2018 Nucl. Fusion **58** 026029
[16] Honda M and Fukuyama A 2006 Nucl. Fusion **46** 580
[17] Morales J et al. 2019 Proc. 46th EPS Conf. Plasma Phys. (Milano) P5.1011
[18] Tani K et al. 1981 J. Phys. Soc. Japan **50** 1726
[19] Hayashi N et al. 2018 27th IAEA Fusion Energy Conf. (Ahmedabad, India, 2018), PPC/1-1
[20] Honda M et al 2018 Nucl. Fusion **58** 112012
[21] Satake S et al 2011 Plasma Phys. Control. Fusion **53** 054018
[22] Hirshman S P et al 1986 Comput. Phys. Commun. **43** 143
[23] Douai D et al 2018 Nucl. Fusion **58** 026018
[24] Wauters T et al. 2019 46th EPS Conf. Plasma Phys. (Milano) I.102, to be submitted to Plasma Phys. Control. Fusion
[25] Farina D 2007 Fusion Sci. Technol. **52** 154
[26] Stober J 2011 Nucl. Fusion **51** 083031
[27] Ricci D et al. 2019 Proc. 46th EPS Conf. Plasma Phys. (Milano) O5.103
[28] Granucci G et al. 2015 Nucl. Fusion **55** 093025
[29] Albanese R, Villone F 1998 Nucl. Fusion **38** 723
[30] Kim H-T et al 2012 Nucl. Fusion **52** 103016
[31] Kobayashi T et al. 2015 Fus. Eng. Des. **96-97** 503
[32] Zoletnik S et al. 2013 Fus. Eng. Des. **88** 1405
[33] Moro A et al. 2017 Fusion Eng. Des. **123** 435
[34] Sozzi C et al. 2019 Proc. 46th EPS Conf. Plasma Phys. (Milano) P4.1089
[35] Urano H et al. 2015 Fus. Eng. Des. **100** 345
[36] Miyata Y et al. 2014 Plasma Fus. Res. **9** 3403045
[37] Cruz N et al. 2017 Control Eng. Practice **63** 81

[38] Albanese R et al. 2015 Fus. Eng. Des. **96-97** 664
[39] Heumann H et al. J. Plasma Physics (2015) **81** 905810301
[40] Pégourié B et al. 2007 Nucl. Fusion **47** 44.
[41] Zagórski R et al. 2016 Nucl. Fusion **56** 016018
[42] Zagórski R et al. 2017 Nucl. Fusion **57** 066035
[43] Gałązka K et al. 2018 Contrib. Plasma Phys. **58** 751
[44] Gałązka K et al. 2017 Plasma Phys. Control. Fusion **59** 045011
[45] Romanelli M et al. 2017 Nucl. Fusion **57** 116010
[46] Kawashima H et al. 2016 Contrib. Plasma Phys. **56** 778.
[47] Hoshino K et al. 2018 Contrib. Plasma Phys. **58** 638
[48] Wiesen S et al. 2015 Journ. Nucl. Mater. **463** 480
[49] Rubino G et al. 2019 Proc. 46th EPS Conf. Plasma Phys. (Milano) P5.1039
[50] Chernyshova M et al. 2019 Proc. 46th EPS Conf. Plasma Phys. (Milano) P1.1012
[51] Vallar M et al. 2019 Proc. 46th EPS Conf. Plasma Phys. (Milano) P5.1008
[52] Varje J et al. 2019 Proc. 46th EPS Conf. Plasma Phys. (Milano) P2.1086
[53] Bierwage A et al. 2019 Plasma Phys. Control. Fusion **61** 014025
[54] Coelho R et al. 2019 Proc. 46th EPS Conf. Plasma Phys. (Milano) P4.1031
[55] Garcia J et al. 2015 Nucl. Fusion **55** 053007
[56] Ayllon-Guerola J et al. 2019 Proc. 46th EPS Conf. Plasma Phys. (Milano) P1.1009
[57] Perelli-Cippo E et al. 2019 Proc. 46th EPS Conf. Plasma Phys. (Milano) P2.1011
[58] Ph. Lauber et al., 2007 Jour. Comp. Phys. **226** 447
[59] Ph. Lauber, 2013 Phys. Reports **533** 33
[60] Borba D et al. 2004 Plasma Phys. Control. Fusion **46** 809
[61] Gassner T et al. 2012 Phys. Plasmas **19** 032115
[62] Girardo J-B et al. 2016 Phys. Plasmas **23** 012505
[63] Vega J et al. 2019 Fus. Eng. Des. https://doi.org/10.1016/j.fusengdes.2019.02.061
[64] Dibon M et al. 2019 Proc. 46th EPS Conf. Plasma Phys. (Milano) P5.1006
[65] Huysmans G, Czarny O 2007 Nuclear Fusion **47** 659
[66] Pamela S et al. 2018 27th IAEA Fusion Energy Conf. (Ahmedabad, India, 2018), OV/4-4
[67] Aiba N et al. 2018 Plasma Phys. Control. Fusion **60** 014032
[68] Futatani S et al. 2014 Nucl. Fusion **54** 073008
[69] Gal K et al. 2008 Nucl. Fusion **48** 085005
[70] Pigatto L et al. 2019 Nucl. Fusion **59** 106028

[71] Albanese R et al. 2008 IEEE Transactions on Magnetics **44** 1654
[72] Pigatto L et al. 2019 Proc. 46th EPS Conf. Plasma Phys. (Milano) P5.1002
[73] Shiraishi J et al. 2017 Nucl. Fusion **57** 126051
[74] Sauter O et al. 2002 Plasma Phys. Control. Fusion **44** 1999
[75] Ramponi G et al. 1999 Phys. Plasmas **6** 3561
[76] Basiuk V et al. 2017 Plasma Phys. Control. Fusion **59** 125012
[77] Nowak S et al. 2019 submitted for publication
[78] Villone F et al. 2013 Plasma Phys. Control. Fusion **55** 095008.
[79] De Tommasi G et al. 2018 27th IAEA Fusion Energy Conf. (Ahmedabad, India, 2018), EX/P3-26
[80] Fukumoto M et al 2017 Phys. Scr. **2017** 014029
[81] Boboc A et al. 2018 Plasma Phys. Control. Fusion **60** 075016
[82] Beeke O et al. 2019 Proc. 46th EPS Conf. Plasma Phys. (Milano) P5.1013
[83] Coda S et al. 2019 Proc. 46th EPS Conf. Plasma Phys. (Milano) P1.1013
[84] Asztalos Ö et al 2017 Fusion Eng. Des. **123** 861.

B_t	2.25 T
I_p	5.5 MA
R / a	2.96 / 1.18 m
A	2.5
κ / δ	1.93 / 0.5
V_p	133 m^3
t (flat-top)	100 s
H&CD power	41 MW
N-NBI (500 keV)	10 MW
P-NBI (85 keV)	24 MW
ECRH (82, 110, 138 GHz)	7 MW

***Table 1**: Nominal parameters of the JT-60SA tokamak. From top to bottom: toroidal magnetic field, plasma current, major and minor radii, aspect ratio, elongation and triangularity, plasma volume, flat-top duration, total H&CD power, negative-ion based neutral beam power (and injection energy), positive-ion based neutral beam power (and injection energy), electron cyclotron heating power (and wave frequencies).*

	#1 Inductive	#2 Inductive	#3 High density	#4-1 ITER-like	#4-2 Advanced Inductive	#5-1 High β Full-CD	#5-2 High β,f_G Full-CD	#6 300s High β
configuration	DN	SN	SN	SN	SN	SN	SN	SN
I_p (MA)	5.5	5.5	5.5	4.6	3.5	2.3	2.1	2.0
B_T (T)	2.25	2.25	2.25	2.28	2.28	1.72	1.62	1.41
q_{95}	3.2	3	3	3.2	4.4	5.8	6	4
P_{add} (MW) $P_{NNB}/P_{PNB}/P_{EC}$	41 10/24/7	41 10/24/7	30 10/20/0	34 10/24/0	37 10/20/7	37 10/20/7	30 6/17/7	13.2 3.2/6/4
$\bar{n}_e$ ($10^{19}m^{-3}$) /f_G	6.3 / 0.5	6.3 / 0.5	10 / 0.8	9.1 / 0.8	6.9 / 0.8	5.0 / 0.85	5.3 / 1.0	2.0 / 0.39
β_N	3.1	3.1	2.6	2.8	3.0	4.3	4.3	3.0

***Table 2**: Main parameters of the JT-60SA reference scenarios. DN, SN: double null, single null configurations.* I_p *: plasma current;* B_T *: toroidal magnetic field;* q_{95} *: safety factor at 95% of the poloidal magnetic flux;* P_{add} *: additional heating power;* P_{NNB} *: negative neutral beams power;* P_{PNB} *: positive neutral beams power;* P_{EC} *: electron cyclotron power;* $\bar{n}_e$ *: line-averaged electron density;* f_G *: ratio of the line-averaged electron density to the Greenwald density;* β_N *: normalised plasma beta.*

f_p (Hz)	$\langle n_e \rangle$ (10^{20} m^{-3}) fuelling only	$\langle n_e \rangle$ (10^{20} m^{-3}) fuelling + pacing
12.5	1.08	1.20
11.1	1.02	1.15
10.0	0.96	1.10
9.1	0.91	1.05
8.3	0.87	1.02
7.7	0.85	1.00

***Table 3**: Simulations with JINTRAC and pellet ablation module HPI2 of discharge evolution during pellet injection for 6 different values of the fuelling pellet frequency f_p (column 1). Volume averaged electron density with pellet fuelling (column 2) and with pellet fuelling and pacing at 50 Hz (column 3).*

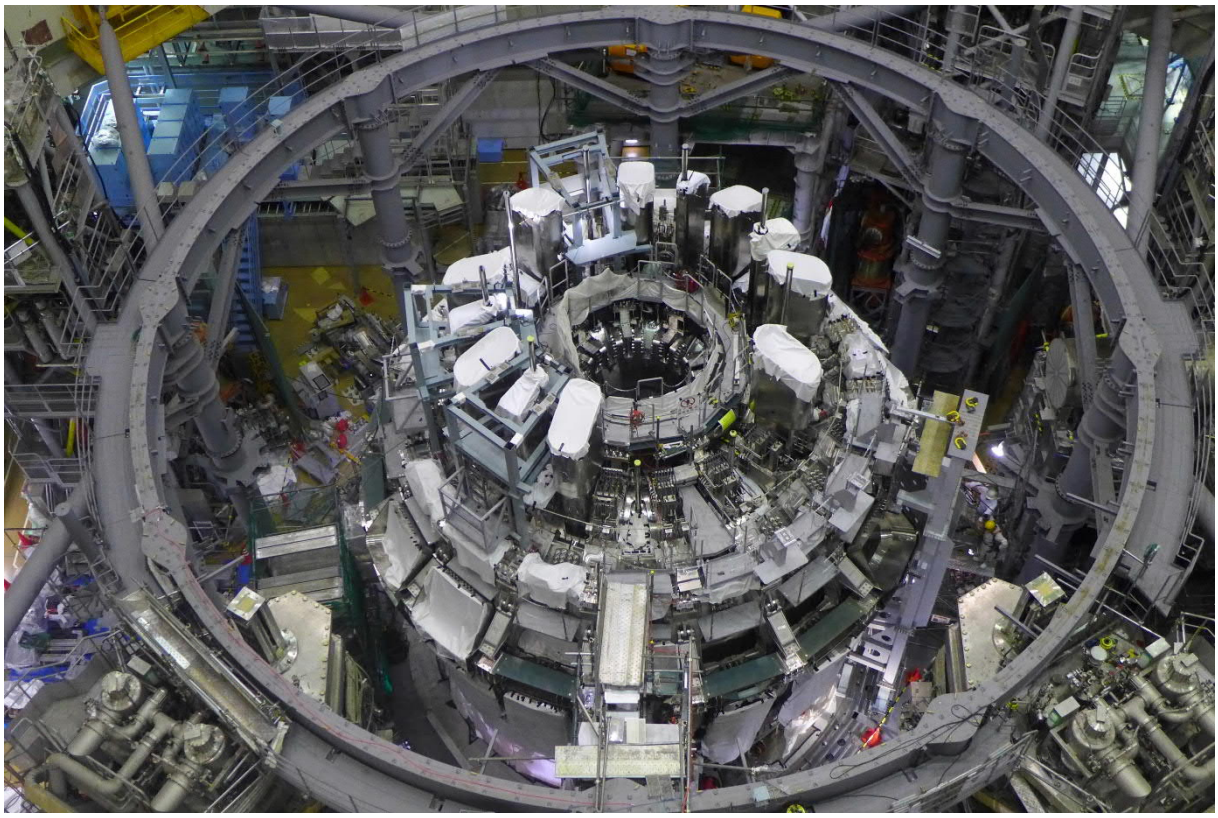

***Fig. 1**: Photograph of JT-60SA, showing the state of assembly in spring 2019*

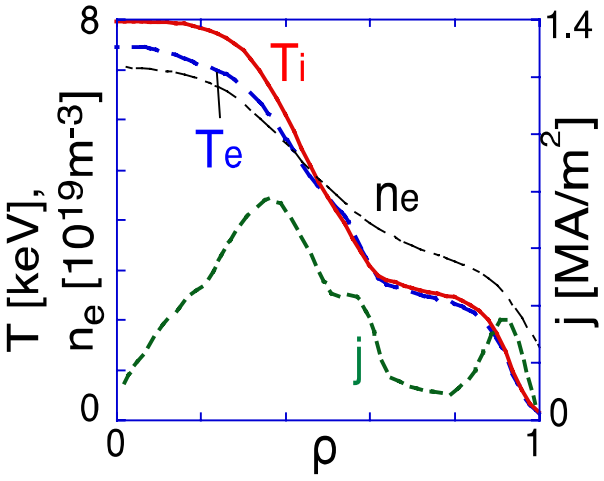

***Fig. 2**: Simulations by the TOPICS code of the stationary phase of Scenario 5-1, but at reduced heating power (26 MW). Profiles of electron density (prescribed), current density, ion and electron temperatures vs radial coordinate ρ (square root of normalised toroidal flux).*

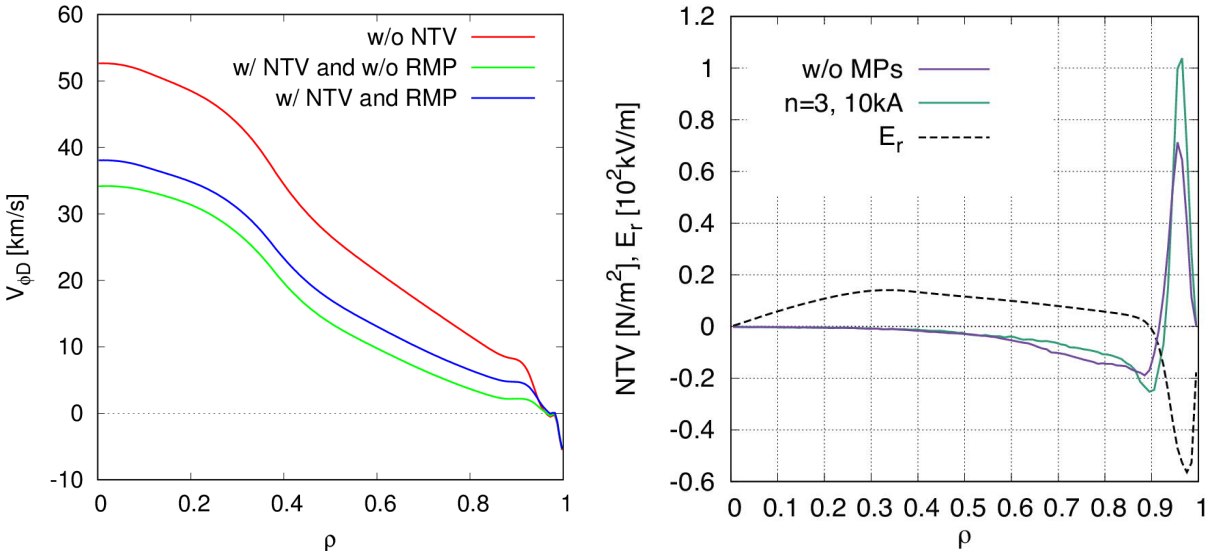

***Fig. 3**: Simulation by means of an integrated modelling framework including the codes TOPICS, OFMC, FORTEC-3D and VMEC for H-mode high current, high density scenario 3. Left: Deuterium ion toroidal velocity profile; all the curves correspond to simulations with the NBI torque; the green curve also includes NTV and the blue curve NTV and RMP (n=3, 10 kA current in each of the EFCC coils). Right: NTV torque, with and without RMP (n=3, 10 kA), and radial electric field.*

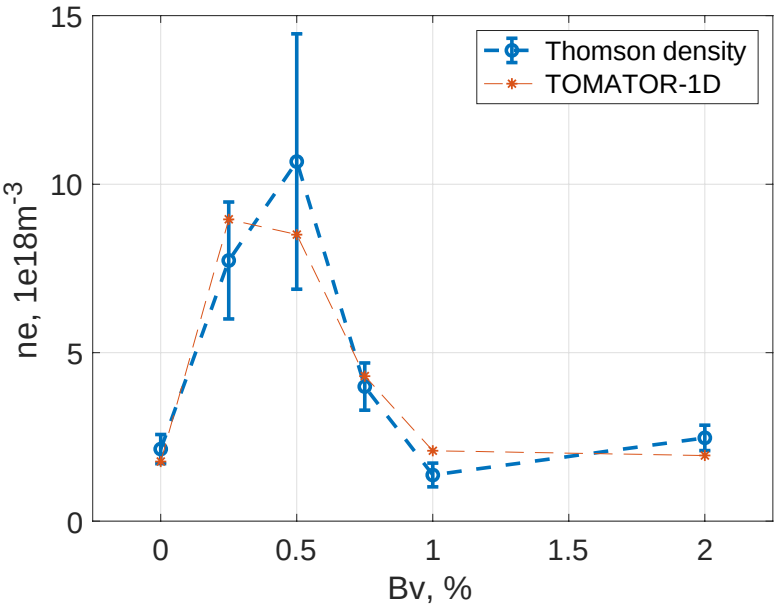

***Fig. 4**: Electron density measured by Thomson scattering and the same quantity simulated by TOMATOR-1D vs vertical magnetic field (in percentage of toroidal field) at $\omega = 2\omega_{c,e}$ for X2-ECRF plasma on TCV at B_t = 1.5T, 400kW of launched power.*

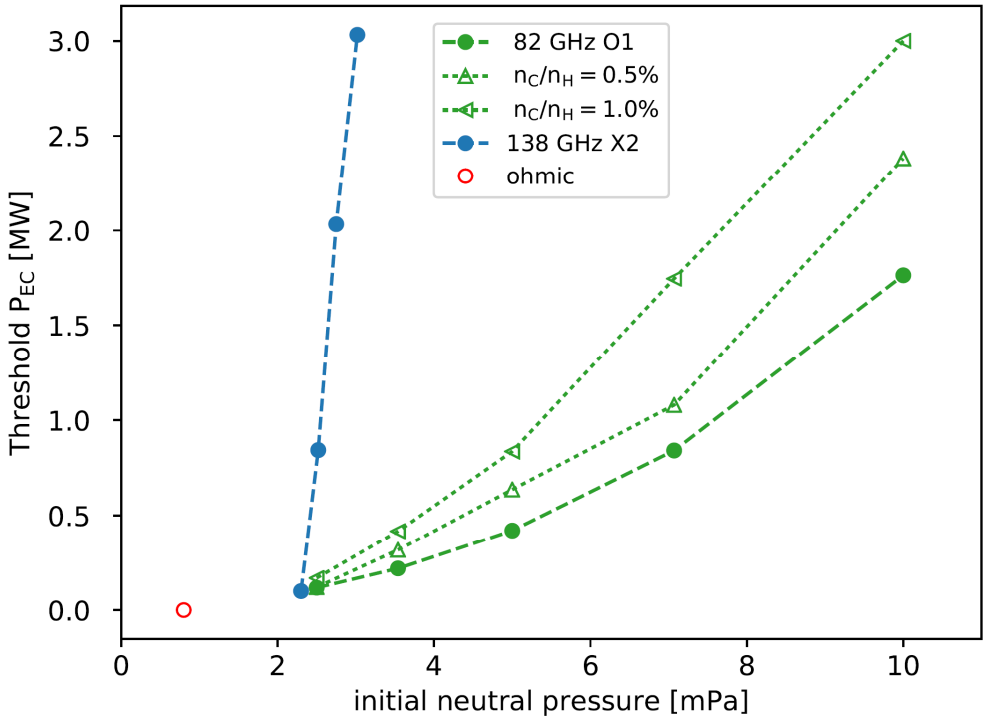

***Fig. 5**: EC assisted breakdown simulation with BKD0, GRAY and CREATE-BD. EC power threshold for successful breakdown as a function of the initial neutral H_2 pressure for 1st harmonic O-mode (optimised injection angles and 2 passes within the breakdown region) and 2nd harmonic X-mode (fixed angles, single pass), at different initial C content and n_O/n_H=0.1%. The red dot represents the ohmic breakdown case.*

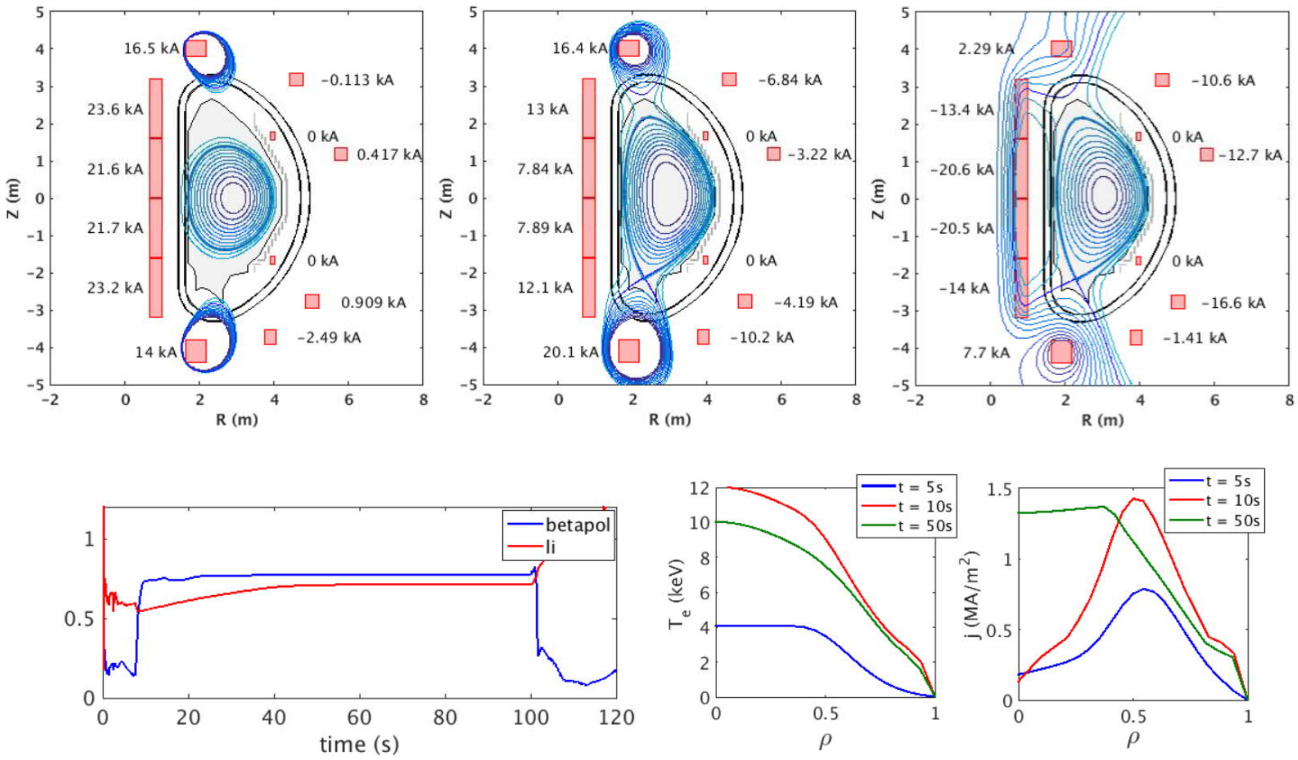

***Fig. 6**: Results of simulations for Scenario 2 (H-mode at plasma current 5.5 MA) combining FEEQS and METIS. Top: snapshots of free boundary equilibria at three different times, from left to right: in the initial phase of the current ramp-up (t = 0.6 s, I_p = 0.5 MA), during the ramp-up (t = 5 s, I_p = 3 MA) and in the flat-top phase (t = 50 s, I_p = 5.5 MA). Bottom: time evolution of β_{pol} and li; electron temperature and current density profiles at different times*

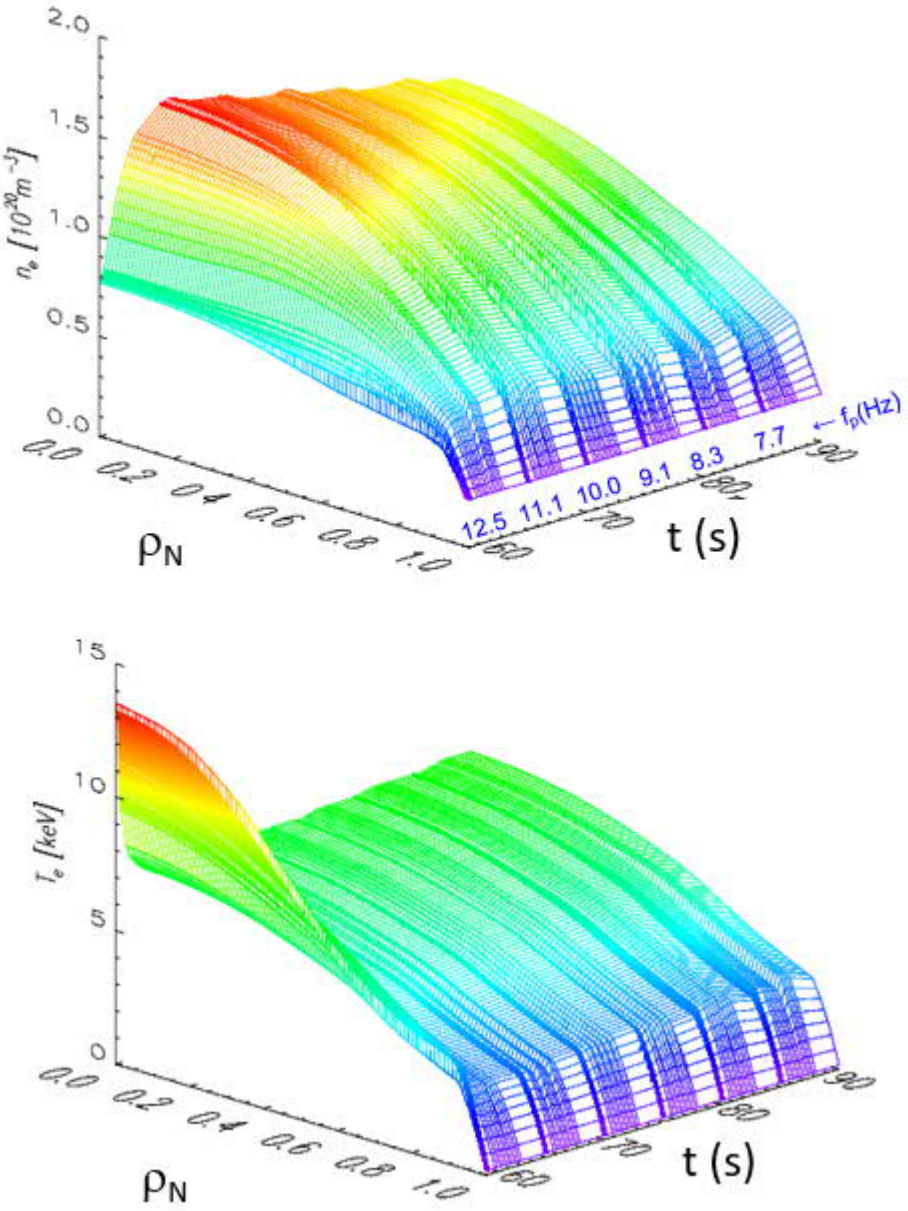

Fig. 7*: Simulations with JINTRAC and pellet ablation module HPI2 of discharge evolution during pellet injection for 6 different values of the fuelling pellet frequency (case with fuelling pellets only). Top: electron density profile vs time and normalised radius. Bottom: electron temperature. The pellets are injected at different frequencies every 5 s, starting from t=60 s.*

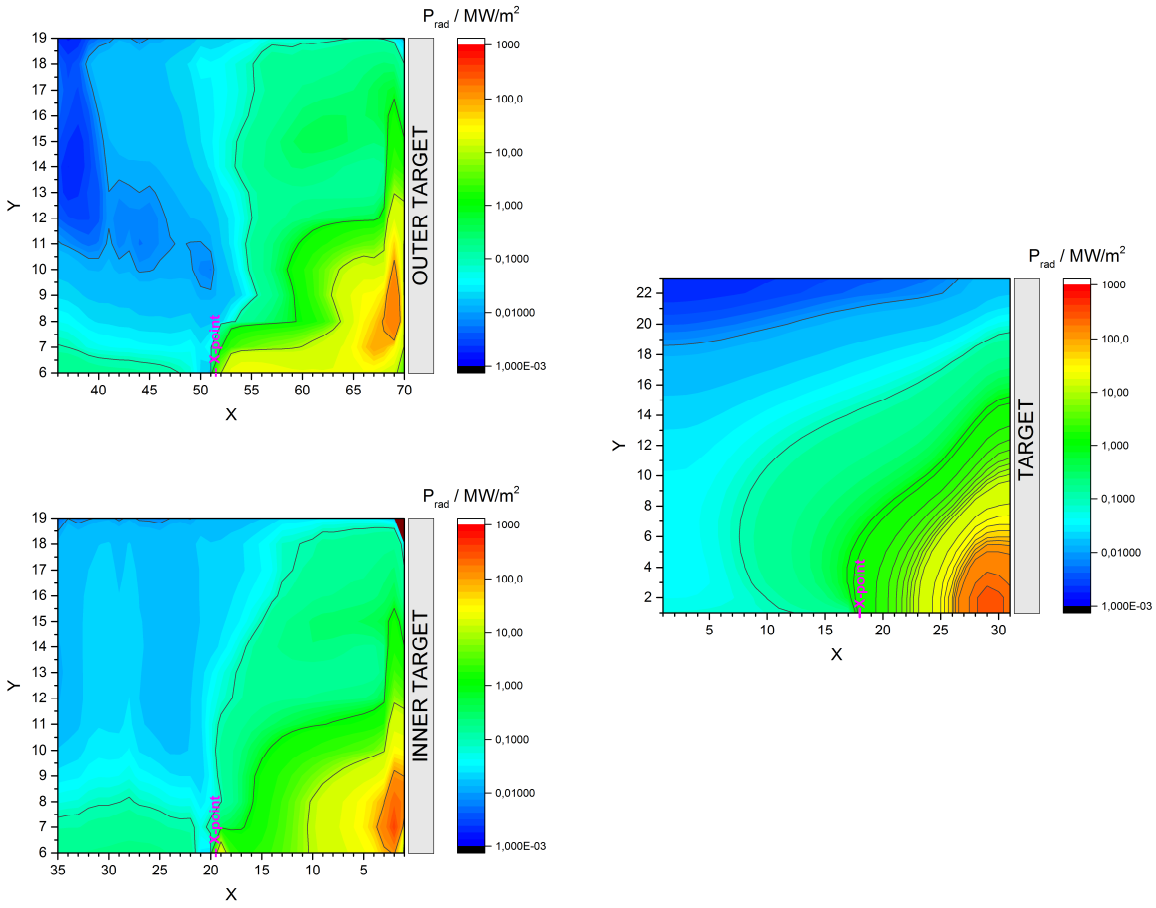

***Fig. 8**: 2D maps of Carbon radiation for Scenario 3 with $n_e^{sep}=2.7\times10^{19}$ m^{-3}. Left: EDGE2D-EIRENE; right: COREDIV. The wall is situated at the top of each graph and the separatrix is at the bottom. The coordinates used are the simulation grid row and column numbers, to facilitate comparison between the two codes, which have different geometries. Note, that in the case of EDGE2D-EIRENE inner target the image is mirrored along column no. 35.*

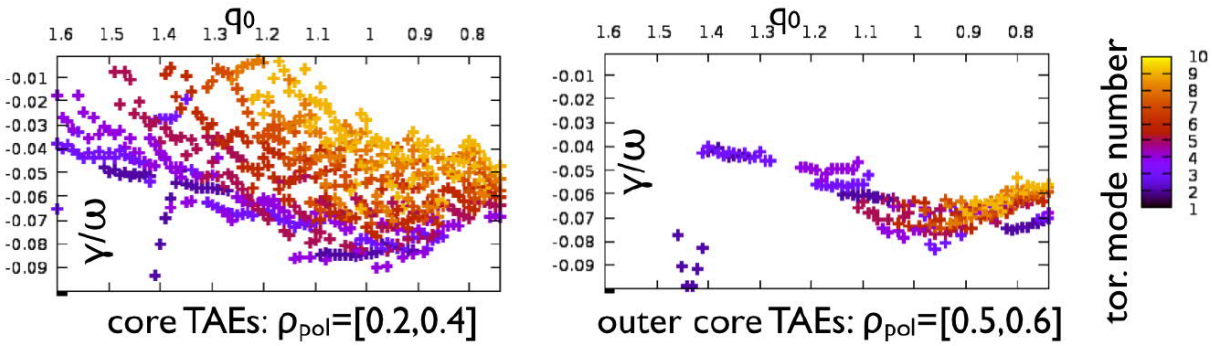

Fig. 9: *damping rates of core (left) and outer core (right) TAEs as a function of q_0 as obtained with the local LIGKA model without EPs. The colors indicate different toroidal mode numbers n=1-10.*

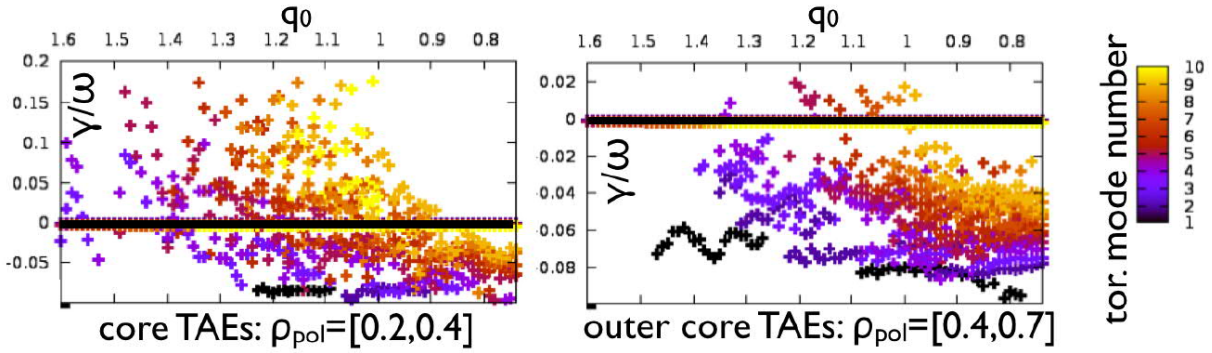

Fig. 10: *growth/damping rates of core (left) and outer core (right) TAEs as a function of q_0 as obtained with the local LIGKA model including EPs. The colors indicate different toroidal mode numbers n=1-10.*

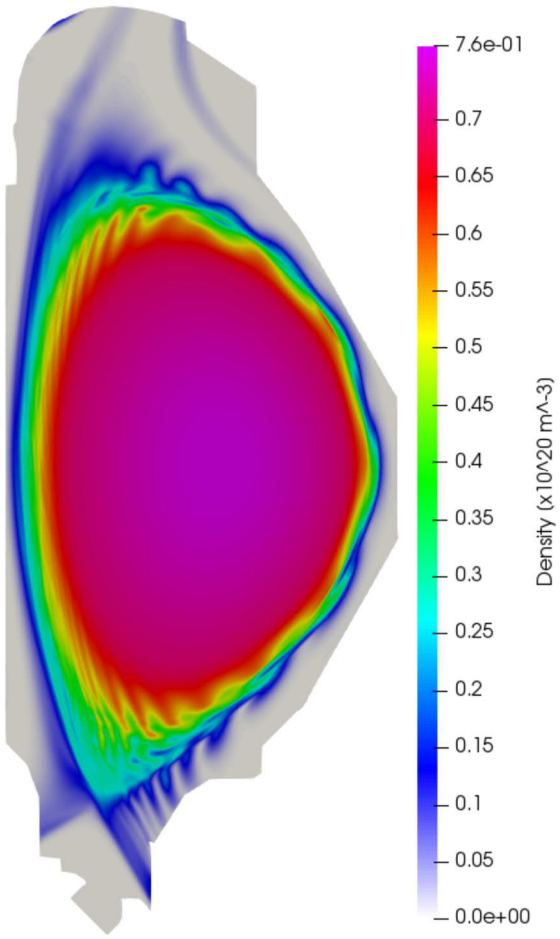

***Fig. 11**: Non-linear MHD simulations by the JOREK code for JT-60SA scenario 4-1. Colour contour plot of the density pattern perturbed by an ELM crash.*

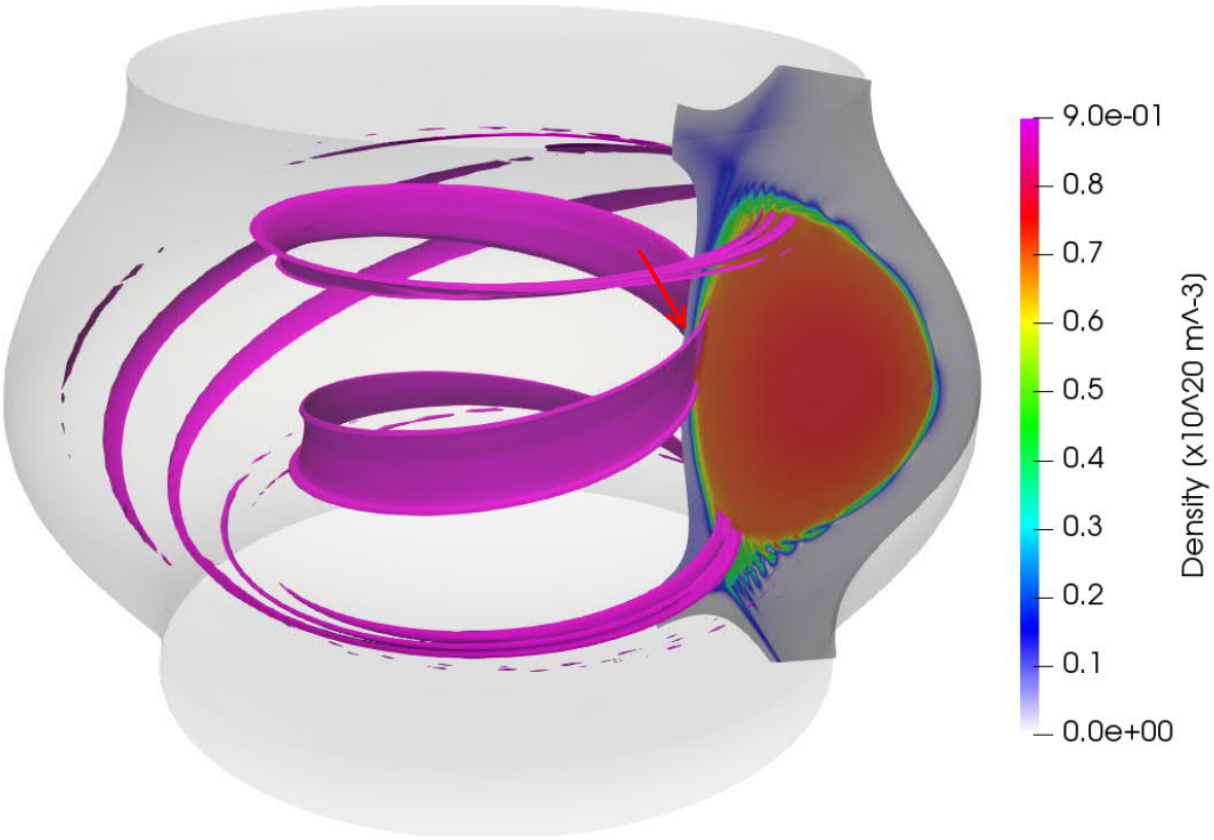

***Fig. 12**: Non-linear MHD simulations by the JOREK code for JT-60SA scenario 4-1: effect of a pellet injection. Colour contour plot of the density pattern perturbed by HFS injected pacing pellet. The red arrow indicates the location of pellet injection.*

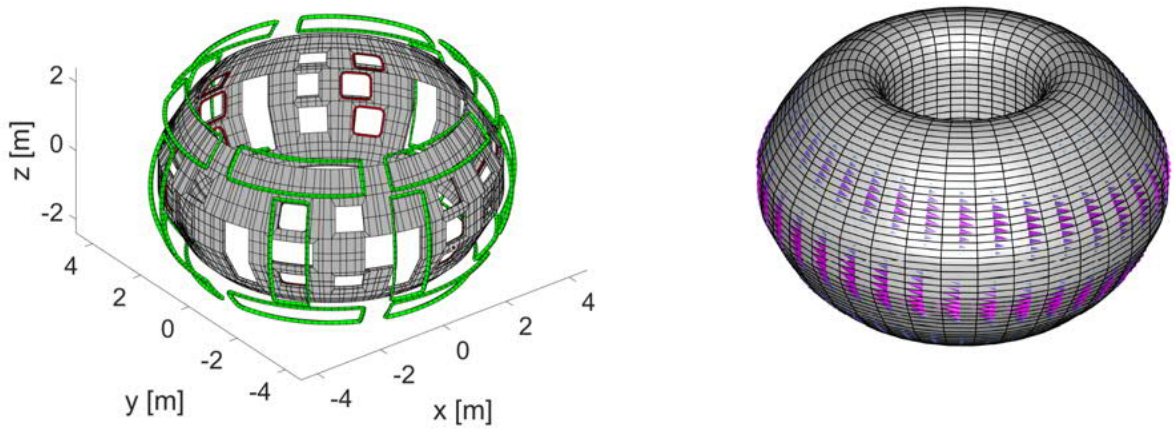

***Fig. 13**: Left: 3D geometry of the stabilising plate (grey), Resistive Wall Mode Control Coils (red) and Error Field Correction Coils (green). Right: CarMa computation of RWM in 3D. Image of the n=1 eigenmode on an axisymmetric surface in the stabilizing plate position.*

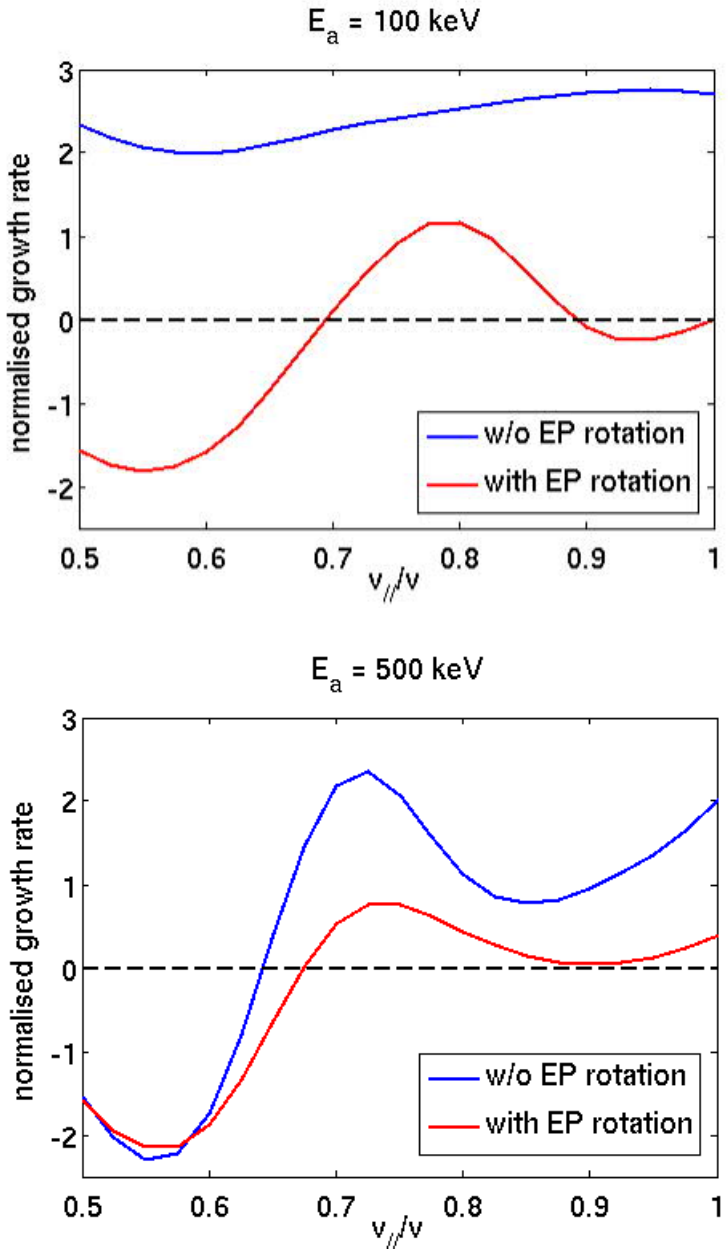

Fig. 14*: Computation of RWM stability by hybrid kinetic-MHD model (MINERVA/RWMaC). Growth rate normalised to the wall decay time vs pitch-angle parameter of the injected Neutral Beam, with and without energetic particle rotation effect. Top: energy of the injected beam E_a = 100 keV. Bottom: E_a = 500 keV.*

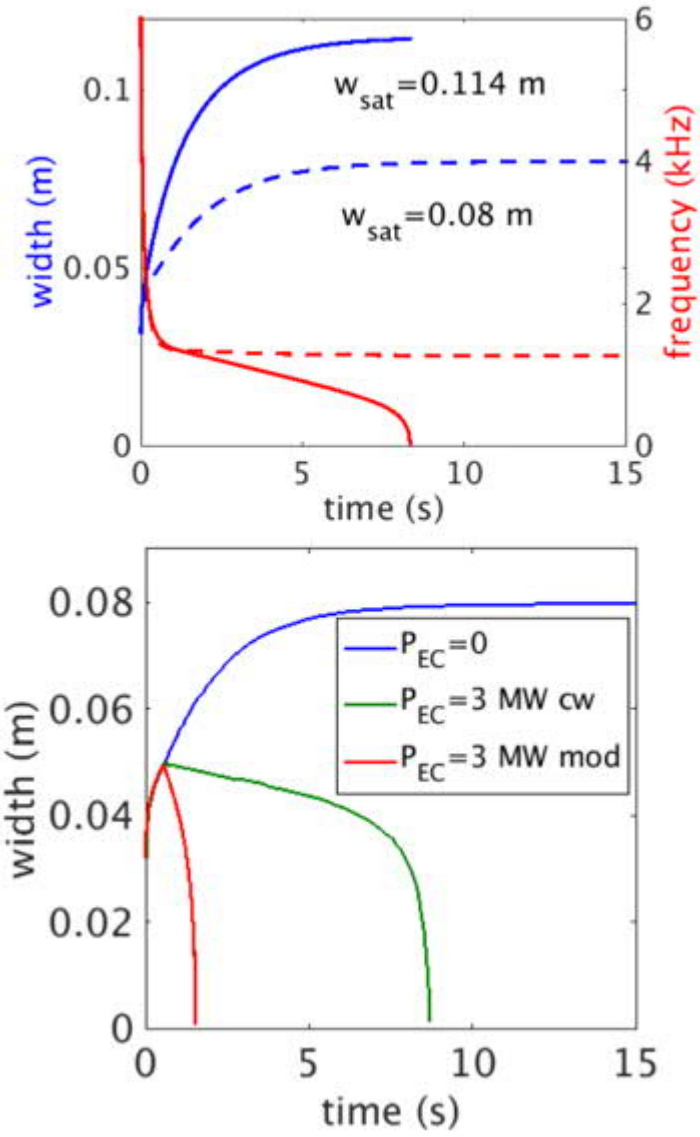

***Fig. 15**: Computation of NTM 2/1 time evolution for scenario 2 parameters. Top: mode width and frequency for Generalised Rutherford Equation parameters corresponding to two different mode saturation widths. Bottom: effect on mode width (w_{sat} = 0.08 case) of 3 MW ECCD, injected continuously (cw) and modulated (mod).*

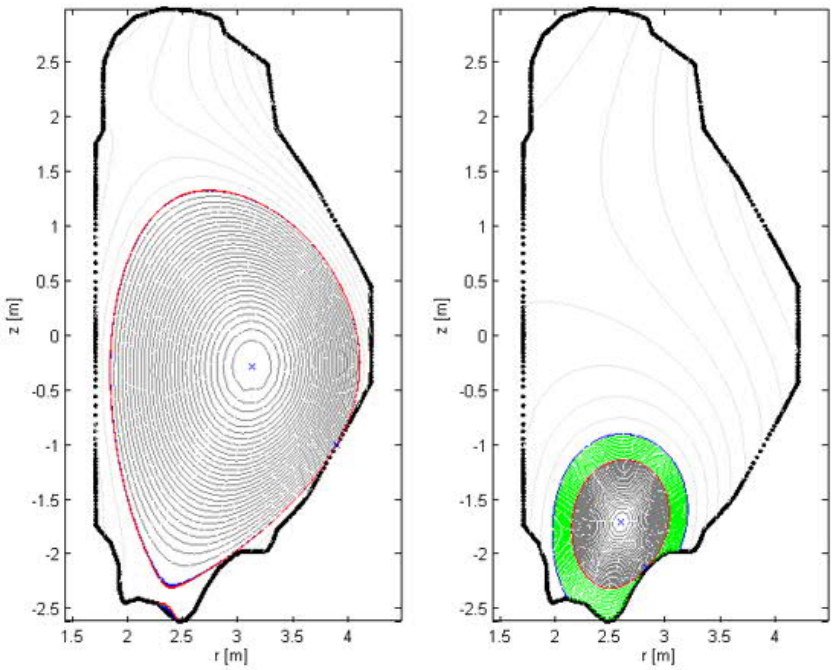

Fig. 16: *Disruption simulation by the CarMa0NL code. Plasma equilibrium configurations during a disruption (downwards VDE); halo currents are shown in green. Left: time at which the plasma hits the wall; right: configuration 5 ms after the start of the CQ. The maximum halo current reaches about 25% of the initial plasma current.*